Rapid Communications | Editors' Suggestion

Salt comets in hand sanitizer: A simple probe of microgel collapse dynamics

Arash Nowbahar,[1] Art O'Connor,[1] Vincent Mansard,[2] Patrick Spicer,[3] and Todd M. Squires[1,*]
[1]*Department of Chemical Engineering, University of California, Santa Barbara, California 93106-5080, USA*
[2]*Laboratory for Analysis and Architecture of Systems, 31400 Toulouse, France*
[3]*School of Chemical Engineering, University of New South Wales, 2052 Sydney, Australia*

(Received 30 September 2017; published 6 June 2019)

Polyelectrolyte microgels find many uses as rheological modifiers and stimulus-responsive materials. Understanding their swelling and collapse dynamics therefore holds broad importance in science and technology. We report remarkably simple experiments, requiring little sophistication, that reveal the subtle physics of microgel collapse. Millimeter-scale bubbles, sugar grains, and other small particles remain suspended and supported by the yield stress of household hand sanitizer, which arises due to a jammed suspension of swollen microgels. By contrast, salt grains with almost identical physical properties sediment through the material, leaving milky "comet tails" behind. Remarkably, the settling speed of a salt crystal remains constant as it dissolves—completely independent of its size or shape until it completely dissolves. Because the settling speed does depend on the type of salt that sediments, we hypothesize that salt grains effectively bore holes through hand sanitizer, with a velocity that is limited by the salt-induced dynamic collapse of the individual microgel particles. A simple convection-diffusion-collapse model successfully relates sedimentation velocities to microgel collapse dynamics for various salts. This model and its predictions are consistent with other observations and with complementary microfluidic experiments.

DOI: 10.1103/PhysRevFluids.4.061301

Polyelectrolyte gels can swell and collapse extensively in response to changing chemical environments [1–4]. This property motivates their use in a range of fields, such as biosensing and drug delivery [5,6], microfluidics [7], musclelike actuators [8], and superabsorbent materials [9]. Colloidal particles made up of polyelectrolytes, called microgels, respond more rapidly to stimuli than bulk gels, and offer additional functionality due to their processability [10,11]. This combination of colloidal and polymerlike characteristics gives rise to distinct properties. For example, a suspension of microgel particles can swell and jam, producing a colloidal glass [12,13].

Jammed, swollen microgel suspensions have a yield stress, meaning they behave as an elastic solid below a critical stress, yet flow as a liquid at higher applied stress. This yield stress can be tuned with changes in concentration, solvent quality, *p*H, and ionic strength [13]. This allows their use in consumer products that can be sprayed, flowed, or poured, yet hold their shape at rest or stick to walls without draining. Hand sanitizer, for example, is a pumpable and spreadable form of alcohol that does not spill from a user's hands, owing to a $\sim$10 Pa yield stress that holds it in place (Fig. 1).

Here, we describe a curious phenomenon that is simple to observe, but which reveals subtle underlying physics. The yield stress of hand sanitizer is strong enough to stably suspend millimeter-scale objects, such as bubbles, sand grains, and sugar crystals (Fig. 1). Despite similar sizes and densities, however, grains of salt slowly fall through hand sanitizer, leaving a cometlike tail (Fig. 2).

*Author to whom correspondence should be addressed: squires@engineering.ucsb.edu

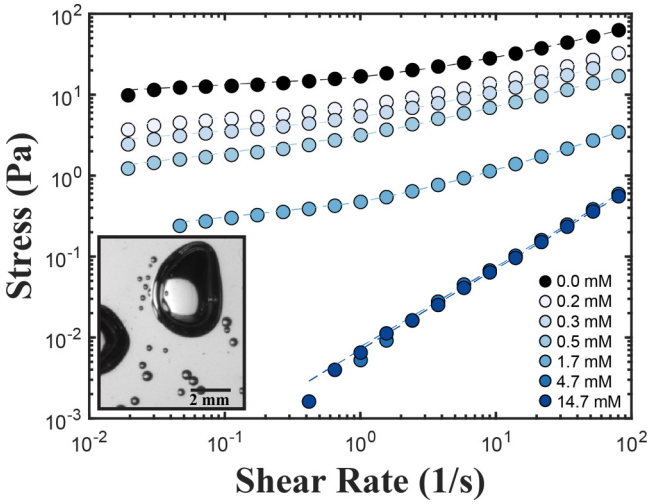

FIG. 1. Steady shear rheology of hand sanitizer shows a finite yield stress $\sigma_Y \sim 10\,\text{Pa}$, which decreases with added [$CaCl_2$], becoming Newtonian above [$CaCl_2$] $\sim$ 2–5 mM. Dashed lines indicate fits to a Herschel-Bulkley model (see Fig. S2 [14]). Inset: Millimeter-sized bubbles remain stably suspended in hand sanitizer, without rising, due to its yield stress.

Despite the simplicity of these experiments, these observations encode subtle information about the microscopic collapse dynamics of microgels, as we describe below.

A force balance determines whether a particle can be supported by a yield stress fluid, or instead sediments through it. To remain suspended, the buoyant weight of an object of volume V_p and buoyant density $\Delta\rho$, given by $V_p\Delta\rho g$, must be smaller than the maximum suspending force that can be exerted by a yield stress σ_y over a contact area A_p. This criterion is often expressed in terms of a dimensionless yield stress Y_g, defined for a particle of radius R by Beris *et al.* [15] to be

$$Y_g = \frac{2\pi R^2 \sigma_y}{\frac{4}{3}\pi R^3(\Delta\rho)g} = \frac{3\sigma_y}{2R(\Delta\rho)g}. \tag{1}$$

A particle sediments through the fluid when the dimensionless yield stress Y_g is sufficiently small, typically $Y_g < 0.14$–0.4 [15,16]. According to this criterion, a 1-mm calcium chloride particle ($\Delta\rho = 1150\ \text{kg/m}^3$) has $Y_g \sim 1.3$ in hand sanitizer, and should not sediment—in direct contrast with our observations. Grains of sugar, whose physical properties are very similar to salt, are indeed

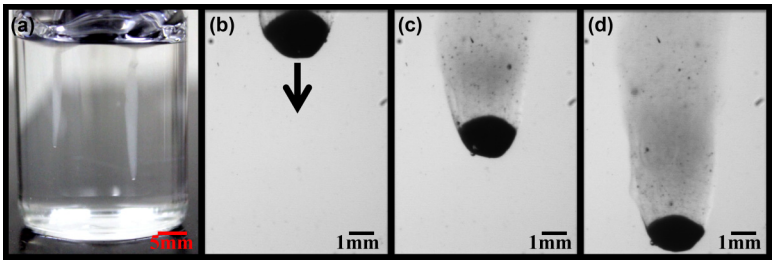

FIG. 2. (a) Snapshot of two sodium chloride particles falling in a vial filled with hand sanitizer. (b)–(d) Closeup snapshots of a calcium chloride particle falling in hand sanitizer, with the arrow indicating the downward direction of motion. Note the cloudy, "comet-tail" streak in the wake of the falling salt grain. (b) $t = 0\,\text{s}$, (c) $t = 40\,\text{s}$, (d) $t = 75\,\text{s}$.

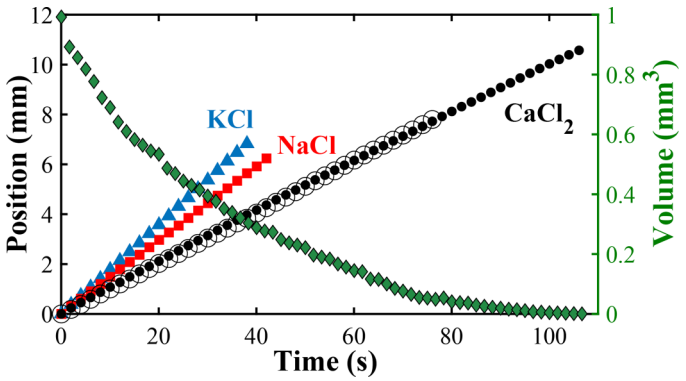

FIG. 3. Position of falling salt grains tracked with time. Triangles, squares, and circles correspond to KCl, NaCl, and $CaCl_2$, respectively. Open circles correspond to a second distinct $CaCl_2$ grain with a significantly different size and shape, showing reproducibility. Diamonds show the volume of the $CaCl_2$ particle corresponding to experiment in solid circles. The sedimentation velocity does not depend on salt grain size (up until complete dissolution), but does depend on salt type.

stably suspended by hand sanitizer. Sedimentation experiments in similar microgel solutions have shown particle sizes necessary for yielding to be much greater than the ∼1-mm salt particle here [17,18].

Even more surprising is that the grain falls with a velocity that remains constant, independent of the grain size, right up to the point where the grain has dissolved completely (Fig. 3). Sedimentation velocities are identical for multiple grains, despite significant variations in size, shape, and roughness. If the microgel were yielding completely, sedimentation velocities should follow Stokes drag, $V = 2\Delta\rho R^2 gA/(9\eta)$, with a correction factor A to account for non-Newtonian behavior [19]. Fall speeds should thus grow with the particle radius squared, in direct contrast to what we observe.

Although the settling velocity does not depend on the particle shape or size, it does depend on the type of salt (Fig. 3), implicating a nonmechanical process. We propose that the salt grain effectively bores a hole through hand sanitizer: As salt dissolves, it collapses the neighboring microgels that had suspended it, thereby making room for the particle to settle downward. Both the salt dissolution and the microgel collapse dynamics may depend on the specific ions comprising the salt. To develop this argument and make it quantitative, we first discuss the microstructure of hand sanitizer, and how it gives rise to the observed yield stress.

The consistency of hand sanitizer is derived from microgel particles of Carbopol, a thickener commonly used in home care and pharmaceutical products over the last 50 years [13,20]. Given enough of a good solvent, each microgel particle would swell to a certain volume. If, however, the microgels are sufficiently concentrated, and too little solvent is available to fully swell all of them, then each swells into its neighbors to form a close-packed, jammed suspension of soft particles [13,21,22]. Jammed microgels must rearrange to flow, which requires a finite force, and therefore a yield stress. In addition to tuning flow properties and suspending particles in consumer products, the yield stress of jammed microgels has been used to stabilize atypical liquid morphologies, e.g., toroidal drops [23] and liquid threads for three-dimensional (3D) printing [24].

Carbopol consists of particles of cross-linked polyacrylic acid (PAA), which deprotonates under certain solvent environments, giving the polymer backbone a negative charge. The phase behavior of such polyelectrolyte networks has been studied extensively, and largely understood through Flory-Rehner gel swelling theories coupled to Donnan theory [4,11,25–28]. The equilibrium size of a microgel is determined by a balance between forces expanding the chains (solvation and ionic) and those contracting them (entropic/elastic). PAA groups deprotonate in good solvents, releasing

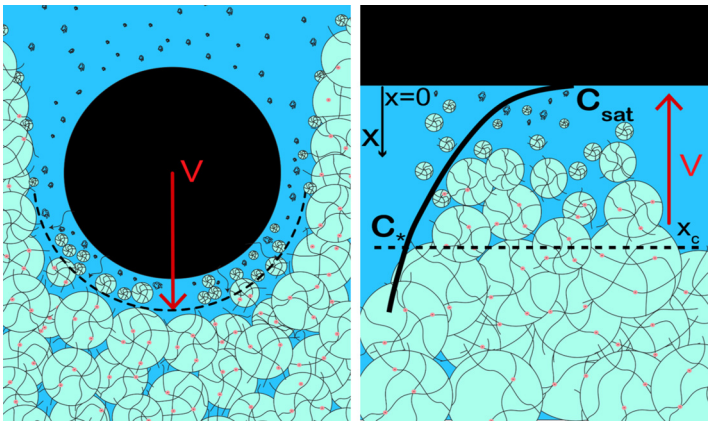

FIG. 4. Proposed mechanism for salt sedimentation through hand sanitizer. Hand sanitizer contains a jammed suspension of soft, swollen Carbopol particles. Dissolving salt diffuses into microgels, collapsing them and removing the yield stress. The particle settles through the fluid, sweeping fluid and collapsed microgels into wake, where they scatter light leaving a "comet tail." The dashed line depicts the location where salt is concentrated enough to begin collapsing microgels. Right: Closeup of the leading edge of the falling grain, in the comoving reference frame, where dissolving salt establishes a steady convection-diffusion boundary layer into the microgel suspension. Microgels start to collapse at x_c, when local concentration exceeds C_* and are advected a distance $x_c = V\tau_c$ during the collapse time.

counterions that remain confined. The higher osmotic pressures draw solvent into the microgel, whose volume may swell a thousandfold, depending on the *p*H [29].

Adding salt to these microgel suspensions screens the charged acrylic acid groups, decreasing the ionic contribution to the total osmotic pressure, and ultimately inducing polymer collapse [30]. In some systems, polyelectrolyte gel swelling/collapse varies smoothly with salt, whereas collapse occurs abruptly in others (e.g., in acetone-water solvent mixtures [3]). When microgels collapse enough to unjam, the fluid loses its yield stress, and the collapsed microgels become suspended, where they diffuse and scatter light.

These features motivate our proposed mechanism for salt sedimentation (Fig. 4): Initially, the gel supports the salt grain without yielding. As salt dissolves, it triggers adjacent microgel particles to collapse, which releases them from the jammed structure. This makes way for the salt crystal to settle downward to the next (uncollapsed, and therefore jammed) microgels. In so doing, the collapsed microgels are swept with the solvent to the rear of the settling particle, where they scatter light to form the "comet tail" trailing the grain. The process repeats continuously until the salt grain has fully dissolved.

We now develop a predictive model for salt settling velocity, constructing scaling arguments based on the mechanism proposed in Fig. 4. In the reference frame moving with the grain, fluid moves upwards with (as yet unknown) velocity V (Fig. 4). Salt dissolves and diffuses away from the grain with diffusivity D, forming a convection-diffusion boundary layer of thickness $\delta \sim D/V$. Assuming $\delta \ll R_s$, and treating the boundary layer as one dimensional, gives a concentration profile

$$C(x) = C_{\text{sat}} \exp\left(\frac{-Vx}{D}\right). \tag{2}$$

Here, C_{sat} is the saturation concentration for the salt in the solvent, which we assume to occur at the surface of the dissolving particle. We assume that microgels begin to collapse when C exceeds some characteristic collapse concentration C_*, which is found at a distance x_c from the grain given by

$$C_* = C_{\text{sat}} \exp\left(\frac{-Vx_c}{D}\right). \tag{3}$$

For the scaling analysis presented here, we do not differentiate between a discontinuous microgel collapse transition that occurs at a specific C_*, or a continuous collapse that happens at a characteristic C_*. Indeed, Ohmine and Tanaka found polyelectrolyte gel swelling to vary continuously with some salts when pure water is the solvent, but discontinuously with salt for acetone/water solvent mixtures [3].

In the comoving frame, microgels begin to collapse when they reach x_c, and must finish by the time they reach the grain surface at $x = 0$. Assuming microgel collapse occurs over a characteristic time τ_c then requires

$$x_c = V\tau_c. \tag{4}$$

Combining Eqs. (4) and (3) then relates the settling velocity to properties of the microgel and salt system, giving

$$V = \sqrt{\frac{D}{\tau_c}}\sqrt{\ln\left(\frac{C_{\text{sat}}}{C_*}\right)}. \tag{5}$$

Equation (5) represents a testable prediction for the settling speed of a particular salt, as it depends on intrinsic material parameters that can be measured or determined in other ways. The saturation concentration C_{sat} is a thermodynamic property of a particular salt in a particular solvent, set by the concentration where the chemical potential of the salt in that solvent is equal to that in its precipitated, solid form, and can be readily measured. Likewise, the salt concentration for collapse C_* follows from Flory-Rehner theory for the particular microgel polymer and salt in the appropriate solvent, and can be determined from equilibrium or rheological measurements (e.g., Fig. 2). Lastly, microgel collapse occurs via diffusive relaxation of polymer chains, which require a time

$$\tau_c = \frac{R_s^2}{\pi^2 D_p}, \tag{6}$$

for microgels of radius R_s and an effective gel diffusivity D_p that depends on the elastic moduli of the microgel and the viscous friction experienced by the gel as solvent is forced through it [11,31]. The R_s^2 dependence has been validated experimentally [11,32], and directly visualized more recently [31,33]. Accordingly, the intrinsic microgel collapse time depends on the chemistry, morphology, and size of the microgel itself, the surrounding solvent, and solute that triggers collapse.

Equation (5) predicts that the salt velocity depends very weakly on the salt concentration at the particle/solution boundary, which in the salt grain experiments is set by C_{sat}. To test the predicted $\sqrt{\ln C}$ dependence, we designed microfluidic experiments [Fig. 5(a)] to systematically vary the salt concentration over several orders of magnitude. Two coflowing streams are introduced into a ~100-μm-tall microfluidic channel: one with hand sanitizer, and the other with a solution of 70 vol % ethanol containing dissolved salt at known concentrations. Each experiment starts when the flow of the hand sanitizer solution is stopped, whereas the alcohol/salt solution remains flowing. The yield stress holds the hand sanitizer in place, and establishes a distinct gel/salt solution interface. Salt diffuses across the interface into the hand sanitizer, collapsing the microgel particles, whereupon the flowing solution shears the collapsed particles away. The interface thus propagates at a velocity set by the collapse front. This geometry allows significant control over the salt concentration, while still capturing the essence of the sedimenting salt experiments. Rather than gravitational sedimentation, however, this configuration uses viscous shear to remove the collapsed microgels and drive the interface forward.

Tracking the salt solution/gel interface [Figs. 5(b)–5(d)] with phase contrast microscopy shows the collapse front to progress linearly in time, with a velocity that depends on $CaCl_2$ concentration [Fig. 5(e)]. A control experiment (black) using a salt-free ethanol/water solution reveals minimal erosion of the microgel, presumably due to weak viscous shear stresses and solvent intrusion between the interstitial spaces of microgel particles. Salt/alcohol solutions, however, cause the interface to erode much more rapidly, and to progress linearly in time (as with the falling salt).

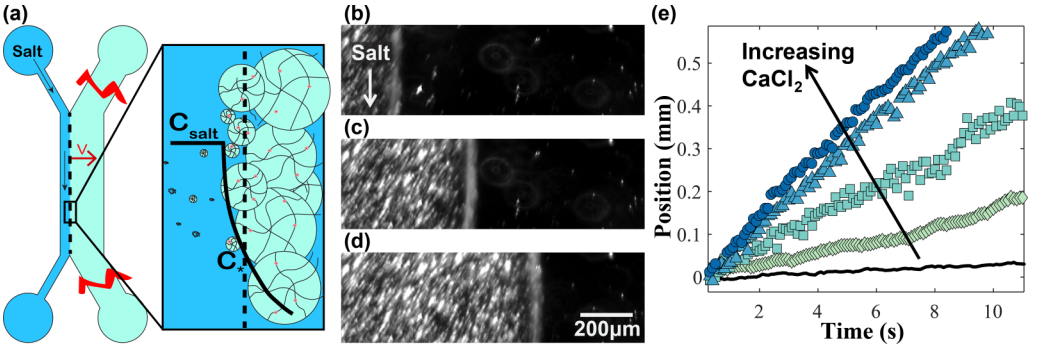

FIG. 5. (a) Schematic of microfluidic experiment. Salt solution is flowed in the left channel, and hand sanitizer flowed in the right channel. The hand sanitizer flow is turned off, with the yield stress holding it in place. The hand sanitizer/solution interface then propagates due to salt-induced collapse, as shown by the zoomed-in inset of the interface. (b)–(d) Phase contrast micrographs of the middle section of the channel at different times when flowing 0.37M $CaCl_2$. Collapsed microgels appear as bright spots. (b) $t = 1$ s. (c) $t = 5$ s. (d) $t = 9$ s. (e) Position of the interface vs time for 70% ethanol mixed with $CaCl_2$ at 2.08M (circles), 0.37M (triangles), 0.032M (squares), 0.016M (diamonds), and 0M (line).

Although the linear progression of the collapse front might resemble case II diffusion of plasticizers into polymers [34], distinct physical mechanisms are responsible for the two different systems. In case II diffusion, solvating or swelling the glassy polymer is the rate-limiting step, and solvent transport through the swollen/plasticized region happens rapidly. Consequently, the swelling front propagates linearly in time, as rapidly as the kinetics of swelling/solvating allow. By contrast, the linear progression of the microgel collapse front—for both settling grains and microfluidic coflows—reflects the convective removal of collapsed microgels by flowing solution. If case II diffusion were responsible, the collapse front would advance linearly with time, even in the absence of flow, e.g., a stationary salt solution in contact with the hand sanitizer. In fact, the collapse front caused by a stationary fluid propagates an order of magnitude more slowly, and moves as $\sim t^{1/2}$ (Fig. S3 [14]). This scaling is inconsistent with case II diffusion, and entirely consistent with diffusion-limited salt transport through an increasingly thick layer of collapsed microgels.

Erosion velocities for different salts at different concentrations increase approximately with $\sqrt{\ln(C)}$ [Fig. 6(a)], as predicted by the proposed diffusive collapse model [Eq. (5)]. Even better agreement is found by introducing the collapse concentration C_* as a free parameter: Best-fit values through the origin reveal V to vary linearly with $\sqrt{\ln(C/C_*)}$, shown as dashed lines. Best-fit values for C_* (11, 14, and 7 mM for KCl, NaCl, and $CaCl_2$, respectively) are broadly consistent with macroscopic measurements of salt concentrations at which the yield stress disappears (e.g., Fig. S2 in the Supplemental Material [14] shows $C_* \sim$ 2–5 mM for $CaCl_2$).

A further consistency check follows when Eq. (5) is rearranged to predict the microgel collapse time,

$$\tau_c = \frac{D}{V^2} \ln\left(\frac{C_{\text{sat}}}{C_*}\right). \tag{7}$$

Experiments with KCl, NaCl, and $CaCl_2$ reveal $\tau_c \sim 0.05$, 0.07, and 0.12 s, respectively (see Supplemental Material [14] for detailed values). It is difficult to determine whether τ_c truly varies with salt type, as implied, given uncertainties in D, C_{sat}, and C_*. However, these timescales are consistent with direct (but rough) microfluidic visualizations of individual microgel collapse dynamics. A monolayer of microgel particles was placed into a microchannel just tall enough to fit the monolayer, and microgel collapse dynamics were followed by phase contrast microscopy (e.g., $\tau_c \sim 0.2$ s for $CaCl_2$, Supplemental Material [14]).

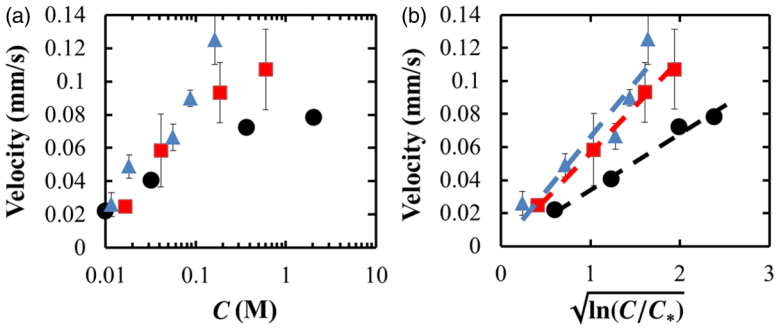

FIG. 6. (a) Velocity of salt solution/microgel interface in microfluidic coflow increases with concentration of KCl (triangles), NaCl (squares), and $CaCl_2$ (circles). (b) Using best-fit values for the microgel collapse concentration C_* reveal a linear relation between the velocity of the microgel/solution interface and $\sqrt{\ln(C/C_*)}$. Dashed lines correspond to linear fits through the origin, with slopes 0.066, 0.057, and 0.034 mm/s. Error bars indicate the standard deviation of at least three replicate experiments, and are smaller than markers when not visible.

As a final consistency check, we use (4) to estimate the distance x_c in front of the grain at which collapse is predicted to occur, finding $x_c = 9$, 11, and 12 μm for KCl, NaCl, and $CaCl_2$, respectively. Video taken with a zoom lens, focusing in front of a sedimenting $CaCl_2$ particle, reveals a region of width $\sim$20 μm where microgels are collapsed and scatter light (see Supplemental Material [14]), broadly consistent with predictions.

In summary, the speed of a salt particle falling through a jammed microgel suspension—a very simple experiment indeed—reveals subtle properties of collapsing microgels. This collapse time for Carbopol would generally be difficult to measure optically, given its optical transparency, high volume fraction, and general difficulty of changing the solution environment with sufficient speed. Further insight into the polymer dynamics follows by combining (6) and (5), relating the sedimentation velocity exclusively to properties of the salt, solvent, and microgel,

$$V = \frac{\pi}{R_s}\sqrt{DD_p}\sqrt{\ln\left(\frac{C_{\mathrm{sat}}}{C_*}\right)}. \tag{8}$$

Estimates for the effective gel diffusivity D_p follow from Eq. (8), given microgel size and salt parameters. Carbopol radii were found to range between 4 and 10 μm in light scattering, scanning electron microscopy (SEM), cryo-SEM, and drag force experiments [13,35]. Our work suggests an upper bound of $\sim$8 μm for R_s (see Supplemental Material [14]). Assuming the middle of this range ($R_s \sim 6$ μm) gives $D_p \sim$ 10–30 $\mu\mathrm{m}^2/\mathrm{s}$, which is consistent with other microgels [11,31,36,37].

Measuring, manipulating, and understanding the dynamics of stimuli-responsive materials is crucial for the ongoing development of various fields and technologies, ranging from 3D printing [24,38], to soft actuators [39]. Our work reveals a connection between the sedimentation of a macroscopic salt grain and the dynamics of polymer diffusion in jammed microgel suspensions. A simple convection-diffusion-collapse model captures the physics of a salt grain sedimenting in a microgel suspension, and suggests that both microscopic (D_p, C_*) and mesoscopic (R_s) characteristics determine the dynamics of microgel systems. These and other insights will continue to inform the design of responsive microgel materials.

We gratefully acknowledge NSF support under Grant No. CBET-1438779, the NSF Graduate Research Fellowship under Grant No. DGE-1144085, use of the Shared Experimental Facilities of the Materials Research Science and Engineering Center at UCSB (MRSEC NSF DMR 1720256), the UCSB Nanofabrication Facility, part of the NSF-funded NNIN network, and the Microfluidics

Laboratory within the California NanoSystems Institute, supported by UCSB and the UC Office of the President. Any opinion, findings, and conclusions or recommendations expressed in this material are those of the authors and do not necessarily reflect the views of the National Science Foundation.

[1] T. Tanaka, Collapse of Gels and the Critical Endpoint, Phys. Rev. Lett. **40**, 820 (1978).
[2] T. Tanaka, D. Fillmore, S.-T. Sun, I. Nishio, G. Swislow, and A. Shah, Phase Transitions in Ionic Gels, Phys. Rev. Lett. **45**, 1636 (1980).
[3] I. Ohmine and T. Tanaka, Salt effects on the phase transition of ionic gels, J. Chem. Phys. **77**, 5725 (1982).
[4] E. Yu. Kramarenko, O. E. Philippova, and A. R. Khokhlov, Polyelectrolyte networks as highly sensitive polymers, Polym. Sci., Ser. C **48**, 1 (2006).
[5] A. J. Grodzinsky and P. E. Grimshaw, Electrically and chemically controlled hydrogels for drug delivery, in *Pulsed and Self-Regulated Drug Delivery*, edited by J. Kost (CRC Press, Boca Raton, FL, 1990), p. 47.
[6] N. A. Peppas, Hydrogels and drug delivery, Curr. Opin. Colloid Interface Sci. **2**, 531 (1997).
[7] D. J. Beebe, J. S. Moore, J. M. Bauer, Q. Yu, R. H. Liu, C. Devadoss, and B.-H. Jo, Functional hydrogel structures for autonomous flow control inside microfluidic channels, Nature (London) **404**, 588 (2000).
[8] D. Kaneko, G. P. Jian, and Y. Osada, Polymer gels as soft and wet chemomechanical systems–an approach to artificial muscles, J. Mater. Chem. **12**, 2169 (2002).
[9] *Modern Superabsorbent Polymer Technology*, edited by F. L. Buchholz and A. T. Graham (Wiley-VCH, New York, 1998).
[10] F. Di Lorenzo and S. Seiffert, Macro- and microrheology of heterogeneous microgel packings, Macromolecules **46**, 1962 (2013).
[11] T. Tanaka and D. J. Fillmore, Kinetics of swelling of gels, J.Chem. Phys. **70**, 1214 (1979).
[12] L. A. Lyon and A. Fernandez-Nieves, The polymer/colloid duality of microgel suspensions, Annu. Rev. Phys. Chem. **63**, 25 (2012).
[13] J. M. Piau, Carbopol gels: Elastoviscoplastic and slippery glasses made of individual swollen sponges. Meso- and macroscopic properties, constitutive equations and scaling laws, J. Non-Newtonian Fluid Mech. **144**, 1 (2007).
[14] See Supplemental Material at http://link.aps.org/supplemental/10.1103/PhysRevFluids.4.061301 for supporting details, data, and videos, which includes Refs. [40–47].
[15] A. N. Beris, J. A. Tsamopoulos, R. C. Armstrong, and R. A. Brown, Creeping motion of a sphere through a Bingham plastic, J. Fluid Mech. **158**, 219 (1985).
[16] H. Emady, M. Caggioni, and P. Spicer, Colloidal microstructure effects on particle sedimentation in yield stress fluids, J. Rheol. **57**, 1761 (2013).
[17] H. Tabuteau, P. Coussot, and J. R. de Bruyn, Drag force on a sphere in steady motion through a yield-stress fluid, J. Rheol. **51**, 125 (2006).
[18] A. M. V. Putz, T. I. Burghelea, I. A. Frigaard, and D. M. Martinez, Settling of an isolated spherical particle in a yield stress shear thinning fluid, Phys. Fluids **20**, 033102 (2008).
[19] R. P. Chhabra, *Bubbles, Drops, and Particles in Non-Newtonian Fluids*, 2nd ed. (CRC Press, Boca Raton, FL, 2006).
[20] S. J. Curran, R. E. Hayes, A. Afacan, M. C. Williams, and P. A. Tanguy, Properties of Carbopol solutions as models for yield-stress fluids, J. Food Sci. **67**, 176 (2002).
[21] N. W. Taylor and E. B. Bagley, Dispersions or solutions? A mechanism for certain thickening agents, J. Appl. Polym. Sci. **18**, 2747 (1974).
[22] F. K. Oppong, L. Rubatat, B. J. Frisken, A. E. Bailey, and J. R. de Bruyn, Microrheology and structure of a yield-stress polymer gel, Phys. Rev. E **73**, 041405 (2006).
[23] E. Pairam, H. Le, and A. Fernández-Nieves, Stability of toroidal droplets inside yield stress materials, Phys. Rev. E **90**, 021002(R) (2014).
[24] C. B. Highley, K. H. Song, A. C. Daly, and J. A. Burdick, Jammed microgel inks for 3D printing applications, Adv. Sci. **6**, 1801076 (2018).

[25] M. Quesada-Pérez, J. A. Maroto-Centeno, J. Forcada, and R. Hidalgo-Alvarez, Gel swelling theories: The classical formalism and recent approaches, Soft Matter **7**, 10536 (2011).
[26] A. Fernández-Nieves, A. Fernández-Barbero, B. Vincent, and F. J. De Las Nieves, Charge controlled swelling of microgel particles, Macromolecules **33**, 2114 (2000).
[27] A. Fernández-Nieves, A. Fernández-Barbero, and F. J. De las Nieves, Salt effects over the swelling of ionized mesoscopic gels, J. Chem. Phys. **115**, 7644 (2001).
[28] A. Fernández-Nieves, A. Fernández-Barbero, B. Vincent, and F. J. De Las Nieves, Osmotic de-swelling of ionic microgel particles, J. Chem. Phys. **119**, 10383 (2003).
[29] Oral Suspensions, Lubrizol Pharmaceutical Bulletin No. 22, Lubrizol Corporation, 2011.
[30] B. R. Saunders and B. Vincent, Microgel particles as model colloids: Theory, properties and applications, Adv. Colloid Interface Sci. **80**, 1 (1999).
[31] I. J. Suárez, A. Fernandez-Nieves, and M. Marquez, Swelling kinetics of poly(*N*-isopropylacrylamide) minigels, J. Phys. Chem. B **110**, 25729 (2006).
[32] T. Budtova and P. Navard, Swelling kinetics of a polyelectrolyte gel in water and salt solutions. Coexistence of swollen and collapsed phases, Macromolecules **31**, 8845 (1998).
[33] J. J. F. Sleeboom, P. Voudouris, M. T. J. J. M. Punter, F. J. Aangenendt, D. Florea, P. van der Schoot, and H. M. Wyss, Compression and Reswelling of Microgel Particles after an Osmotic Shock, Phys. Rev. Lett. **119**, 098001 (2017).
[34] C. Y. Hui, K. C. Wu, R. C. Lasky, and E. J. Kramer, Case-II diffusion in polymers. II. Steady-state front motion, J. Appl. Phys. **61**, 5137 (1987).
[35] J. Y. Kim, J. Y. Song, E. J. Lee, and S. K. Park, Rheological properties and microstructures of Carbopol gel network system, Colloid Polym. Sci. **281**, 614 (2003).
[36] L. Bromberg, M. Temchenko, V. Alakhov, and T. A. Hatton, Kinetics of swelling of polyether-modified poly(acrylic acid) microgels with permanent and degradable cross-links, Langmuir **21**, 1590 (2005).
[37] *Microgel Suspensions: Fundamentals and Applications*, edited by A. Fernandez-Nieves, H. M. Wyss, J. Mattsson, and D. A. Weitz (Wiley-VCH, Weinheim, 2011).
[38] J. A. Lewis, Direct ink writing of 3D functional materials, Adv. Funct. Mater. **16**, 2193 (2006).
[39] L. Ionov, Hydrogel-based actuators: Possibilities and limitations, Mater. Today **17**, 494 (2014).
[40] D. R. Vogus, V. Mansard, M. V. Rapp, and T. M. Squires, Measuring concentration fields in microfluidic channels *in situ* with a Fabry-Perot interferometer, Lab Chip **15**, 1689 (2015).
[41] S. P. Pinho and E. A. Macedo, Solubility of NaCl, NaBr, and KCl in water, methanol, ethanol, and their mixed solvents, J. Chem. Eng. Data **50**, 29 (2005).
[42] Y. C. Chang and A. S. Myerson, The diffusivity of potassium chloride and sodium chloride in concentrated, saturated, and supersaturated aqueous solutions, AIChE J. **31**, 890 (1985).
[43] W. M. Haynes, *CRC Handbook of Chemistry and Physics*, 97th ed. (CRC Press/Taylor & Francis, Boca Raton, FL, 2016).
[44] M. Capobianchi, T. F. Irvine, Jr., N. K. Tutu, and G. Alanson Greene, A new technique for measuring the Fickian diffusion coefficient in binary liquid solutions, Exp. Thermal Fluid Sci. **18**, 33 (1998).
[45] V. Vitagliano and P. A. Lyons, Diffusion coefficients for aqueous solutions of sodium chloride and barium chloride, J. Am. Chem. Soc. **78**, 1549 (1956).
[46] L. A. Philip and J. F. Riley, Diffusion coefficients for aqueous solutions of calcium chloride and cesium chloride at 25°, J. Am. Chem. Soc. **76**, 5216 (1954).
[47] D. Bartolo, G. Degré, P. Nghe, and V. Studer, Microfluidic stickers, Lab Chip **8**, 274 (2008).